Proceedings of the ASME 2024
International Design Engineering Technical Conferences and
Computers and Information in Engineering Conference
IDETC/CIE 2024
August 25-28, 2024, Washington, DC

DETC2024/CIE-141866

SYMMETRY-INDUCED MECHANICAL METAMATERIALS DESIGN FRAMEWORK AND DATASET GENERATION

Mohammad Abu-Mualla, Jida huang*

Department of Mechanical and Industrial Engineering, University of Illinois at Chicago, Chicago, Illinois 60607

ABSTRACT

The surge in machine learning research and recent advancements in 3D printing technologies have significantly enriched materials science and engineering, particularly in the domain of mechanical metamaterials, which commonly consist of periodic truss materials. Despite the extensive exploration of their tailorable properties, truss-based metamaterial design has predominantly adhered to cubic and orthotropic unit-cells, a limitation arising from the conventional design method, where the type of symmetry related to the designed truss-based material is determined after the design process is done. To overcome this issue, this work introduces a groundbreaking 3D truss material designing framework that departs from this constraint by employing six distinctive material symmetries (cubic, hexagonal, tetragonal, orthotropic, trigonal, and monoclinic) within the design process. This innovative approach represents a versatile paradigm shift compared to previous design approaches. Furthermore, we are able to integrate anisotropy into the design framework, thus enhancing the property space exploration capability of the proposed design framework. Probing materials property space using our design framework demonstrates its capacity to achieve a diverse range of mechanical properties, surpassing even the most extensive datasets available in the literature. The proposed method facilitates the generation of a comprehensive truss dataset, which can be represented in a trainable continuous format suitable for machine learning and data-driven approaches. This advancement paves the way for the development of robust inverse design tools for truss materials, marking a significant contribution to the mechanical metamaterial community.

1. INTRODUCTION

Architected metamaterials, propelled by inspiration from crystallographic networks, tailored microstructural design, and additive manufacturing, are reshaping the realm of attainable material properties, marking an era of unparalleled functionality [1–3]. In crafting periodic cellular structures, a meticulous approach

entails precise control over the architecture of repeating unit-cells [3, 4]. This intentional design process yields cellular structures capable of advanced macroscopic mechanical properties, including negative Poisson's ratios [5, 6], remarkable strength-to-weight ratios [7, 8], and controlled instabilities [9, 10]. These cellular materials have also applications across a wide spectrum of phenomena, ranging from counter-intuitive negative compressibility [11] to mechanical cloaking [12], extreme energy absorption [13, 14], and guided acoustic waves [15, 16]. Truss materials are widely recognized for their extensive use among available cellular material designs, primarily due to their straightforward manufacturing process and remarkable strength-to-weight ratios [7, 8]. The attractive features of truss metamaterials lie in the huge design flexibility influenced by both lattice topology (dictated by beam network connectivity) and geometric features (dictated by the length, orientation, and cross-sectional shape of individual strut).

Despite the vast potential for exploration, a significant portion of truss structures' design space remains unexplored. Numerous designs have adhered to a small, well-established lattice catalog, where the primary focus has been on modifying representative catalog geometrical parameters. Identifying these catalogs typically occurs through trial and error, limiting the scope of potential design variations [17, 18]. Moreover, its potential is significantly constrained in terms of topological tunability, thereby limiting the achievable properties of the families cataloged in the related catalog. Several truss optimization solutions have embraced deterministic and heuristic search strategies to uncover extreme structures, iteratively adjusting active topological elements within the design domain based on mechanics-based criteria [19, 20]. While pure topology optimization approaches have the potential to introduce novel extreme truss material, they often come with computational complexities, particularly in threedimensional (3D) scenarios. These challenges encompass high computational costs and issues such as nonuniqueness and sensitivity to the starting point of the solutions [21]. Furthermore, discovering genuine extreme designs in truss structures is chal-

^{*}Corresponding author: jida@uic.edu

lenging for large-scale design endeavors due to the multitude of possible topological and geometrical configurations and their intricate mechanical and physical interrelations [1]. In addressing these hurdles, recent advancements in computational data-driven approaches [22–25] offer a means to navigate the intricacies of truss structure design space. This is achieved by predicting structures from models that are trained on a parametrized training dataset through applying geometric modification on well-studied unit-cells encompassing different topologies, resulting in a more spread exploration of the design space [22–24]. However, exploring novel structures using data-driven methods requires a design space that encompasses a wide range of topologies, including novel and extreme designs.

To address the limited design and property space challenge, Lumpe and Stankovic have recently presented an extensive catalog of truss lattices inspired by the molecular structure of crystalline lattices [1]. However, a persistent issue arises from the diverse topologies inherent in these designs, making them challenging to effectively represent for machine learning purposes due to their disjoint design space. While Lumpe and Stankovic's designs can be expressed in voxel format, this format is sensitive to shape completion and connectivity issues stemming from the noisy design space intrinsic to voxel representation. On top of that, voxel representation requires resource-intensive computational power, the same as topology optimization methods.

A method for generating a continuous dataset and creating new structures independent of a single catalog is influenced by leveraging crystallographic material symmetries [2, 26]. In contrast to the conventional design approaches where truss materials are designed first, followed by attempts to understand their mechanical behavior through the utilization of material symmetries, the mentioned resource pioneers a reverse process as the design concept is inspired by material symmetry or directional forces within the material. These symmetries resulted in the creation of Cubic and Orthotropic continuous datasets [2, 26]. However, the proposed method in the previous study doesn't include other highly anisotropic materials. It overlooks coupling components like shear-normal and shear-shear in the effective stiffness tensor, even though it's acknowledged that these components could be beneficial for tasks such as compliance minimization and wave guidance [27, 28]. Therefore, there is an urgent need for a method that can create a truss dataset with a continuous design space. The dataset should be in a format that avoids the computational challenges linked to machine learning. This format facilitates the inclusion of various new designs, supports many representations, and encompasses a wide mechanical property space. The data generation method should be easily implemented by other designers, eliminating the need for trial and error in design space exploration.

To bridge the gaps above, we introduce a systematic approach to generate a diverse truss dataset that spans from cubic unit-cells to highly anisotropic structures. The proposed method utilizes the different material planes of symmetry defined in the science of crystallography, allowing for the creation of symmetrical configurations within the dataset. This not only enhances the parameterization of the generated data but also provides a foundation for exploring the influence of symmetry on structural

properties. Then, we introduce sources of anisotropies that eliminate the symmetries from the generated structures. Subsequently, we extend the versatility of our data generation approach, which enables a more comprehensive exploration of truss structures and their diverse characteristics in materials science and engineering applications. The approach permits multiple representations for data-driven methodologies; each truss lattice can naturally be characterized as a graph—a mathematical construct comprising edges and nodes, representing struts and their intersections, respectively. Alternatively, it can be encoded as a parametric representation where representative parameters can fully encode each truss. This method also opens the door for exploring cellular materials beyond the truss-based approach, where other mechanical metamaterials can be integrated. Our contribution can be summarized as follows:

- Develop a systematic approach inspired by the planes of symmetry from crystallography to generate a highly diverse and representative dataset.
- The proposed approach enables multiple representations that can be seamlessly integrated with data-driven methods.
- The approach illuminates the sources of anisotropy in truss materials and elucidates how symmetry planes influence the mechanical properties of truss materials.

The rest of the paper is structured as follows: Section 2 provides a comprehensive review of the literature concerning methods in truss materials generation, exploration of mechanical symmetry, and materials properties computation. Section 3 delves into the methodology of truss construction. In Section 4, we showcase simulation samples and the space of properties of the samples. Sources of anisotropies are elucidated in Section 5. Finally, Section 6 concludes the paper by discussing contributions and limitations and outlining future research directions.

2. LITERATURE REVIEW

This section first introduces the methods typically employed in creating truss datasets. Then, an overview of material symmetries crucial for dataset generation is presented. Lastly, a brief discussion on the homogenization method used to extract the effective mechanical properties from the truss materials concludes this section.

2.1 Truss Dataset Generation

Cellular material frequently employ trusses and beams due to their easy specification and extensive variability. The diversity of truss topologies alone warrants a dedicated classification of truss unit-cells, without even considering continuous parameters such as vertex positions or thickness profiles along beams and their junctions [26]. The exploration of this extensive space has been extensively documented in the literature, focusing on expanding the boundaries of property space by trying to achieve extreme unit-cells [29–31]. The surge in machine learning usage has underscored the need for alternative methods to generate datasets with a broader range of properties. Introduced in 1995, a technique constructs truss microstructures with 2000 potential members, optimizing thicknesses for desired properties using

predetermined elasticity tensors [32]. In their work [22], Chen et al. employed discrete sampling and continuous optimization to generate five catalogs of unit-cells with extreme properties. These catalogs form the basis for their dataset, which is expanded by modifying the truss diameter. Bastek et al. [23] deformed and superimposed seven fundamental lattice units to create 262 topologies. They further diversified the dataset by applying rotations and expansions on the unit-cells. In [33], a cubic dataset was developed, inspired by two representative unit-cell types and other geometric parameters. A recent procedural graph approach succinctly represents the construction process of cellular materials, including truss materials, using a skeleton annotated with spatially varying thicknesses of the truss and bar [34]. This study builds upon two foundational works in data generation, both leveraging material symmetry. The first, [2], employed nine cubic symmetry planes, while [26] utilized three orthogonal planes for orthotropic material. In each method, topologies (nodes and connections) and geometries (cross sections, orientations, etc.) can be manipulated to explore the property space defined by these symmetry planes. While all methods have limited property space coverage, the dataset inspired by crystallography proposed by [1] covered the widest range. However, it lacks a trainable representation that demands less computational power.

2.2 Material Symmetry

Material symmetry refers to the change in properties concerning direction at a specific point in a material [35, 36]. In this study, when discussing symmetry, we specifically mean mirror symmetry. Mirror symmetry occurs when two identical geometric objects are symmetric with respect to a plane, meaning each point on one object has a corresponding symmetric point on the other object concerning that plane [37]. Symmetry planes significantly impact truss material mechanics, notably in determining the stiffness tensor [38], a mathematical representation of a material's response to external forces, capturing its anisotropic behavior [39]. Anisotropy arises when the material exhibits different mechanical properties along distinct axes, and symmetry planes contribute significantly to this phenomenon [36]. In the context of cellular materials, symmetry planes introduce a level of predictability and order to the distribution of forces within the structure. These planes act as reference surfaces, enabling a systematic analysis of the material's response to various loading conditions [2, 26, 36]. Materials are classified into seven anisotropic symmetries based on symmetry planes' number and orientation: triclinic, monoclinic, trigonal, orthotropic, hexagonal, tetragonal, and cubic [37, 40]. Table 1 illustrates these symmetries, including orientation (defined by the Normal to the symmetry plane), the number of symmetry planes, and the count of independent elastic parameters within the stiffness tensor. For a detailed explanation of the derivation of independent elastic parameters, readers can refer to [36], the source from which Table 1 originated.

In Table 1, i_1 , i_2 , and i_3 represent the normal to the three primary planes of the cube. By examining the symmetries from Table 1, researchers and engineers gain insights into how the material responds to external stimuli, intricately tied to its underlying symmetrical characteristics. Therefore, we will use these

TABLE 1: MATERIAL SYMMETRY TYPES AND ITS CHARACTERISTICS.

Type of material symmetry.	Number of planes of mirror symmetry.	Number of independent elastic coefficient	Normals to the plane of symmetry.
Cubic	9	3	$i_1, i_2, i_3, (1/2)(i_1 + i_2), (1/2)(i_1 - i_2), (1/2)(i_1 + i_3), (1/2)(i_1 - i_3), (1/2)(i_2 + i_3), and (1/2)(i_2 - i_3)$
Hexagonal	7	5	$i_1, i_2, i_3, (1/2)(3i_1 + i_2), (1/2)(3i_1 - i_2), (1/2)(i_1 + 3i_2), and (1/2)(i_1 - 3i_2)$
Tetragonal	5	6 (7)	$i_1, i_2, i_3, (1/2)(i_1 + i_2),$ and $(1/2)(i_1 - i_2)$
Orthotropic	3	9	i_1, i_2, i_3
Trigonal	3	6 (7)	i_1 , $(1/2)(i_1 + 3i_2)$, and $(1/2)(i_1 - 3i_2)$
Monoclinic	1	12 (13)	i_1
Triclinic	0	21	None

symmetries further to explore the space of properties achievable with truss materials.

2.3 Effective Mechanical Properties Calculations

Numerical homogenization is a computational approach widely utilized for determining the homogenized macroscopic mechanical properties, specifically the elasticity tensor, of cellular materials [41, 42]. The rationale for selecting the elasticity tensor as a representation of effective mechanical properties lies in the feasibility of obtaining all elastic terms through common approximation methods, such as the Voigt-Reuss-Hill method (VRH) [43], which relies on the elastic stiffness tensor. Numerical homogenization involves the computation of the elasticity tensor using Eq. (1), where E_{ijpq} denotes the stiffness tensor, Ω stands for the volume of the cellular material, ϵ_{ij} is the macroscopic displacement within the virtual displacement field, $\epsilon_{pq}^{0(kl)}$ indicates the prescribed macroscopic displacement, and ν represents the virtual displacement field. The unknown variable we seek to solve for is χ^{kl} . For 3D cellular materials, Eq. (1) must be solved under six distinct independent load cases, defining six prescribed deformations—three axial and three shear deformations. A comprehensive explanation of this method is available in the reference [41].

$$\int_{\Omega} E_{ijpq} \, \epsilon_{ij}(\nu) \, \epsilon_{pq}(\chi^{kl}) \, d\Omega = \int_{\Omega} E_{ijpq} \, \epsilon_{ij}(\nu) \, \epsilon_{pq}^{0(kl)} \, dV \quad \forall \, \nu \in \Omega$$
 (1)

3. METHODOLOGY

This section includes two subsections: Sec.3.1 delves into the framework of the utilization of symmetry planes in the design of truss material topologies. Sec.3.2 discusses the continuity and the constraints that are put in place to ensure the connectivity of the truss structure.

3.1 Design Framework

Our focus is on lattices derived from the periodic tessellation of a cubic representative volume element (RVE). Drawing inspiration from the cube decomposition approach [2, 26], we

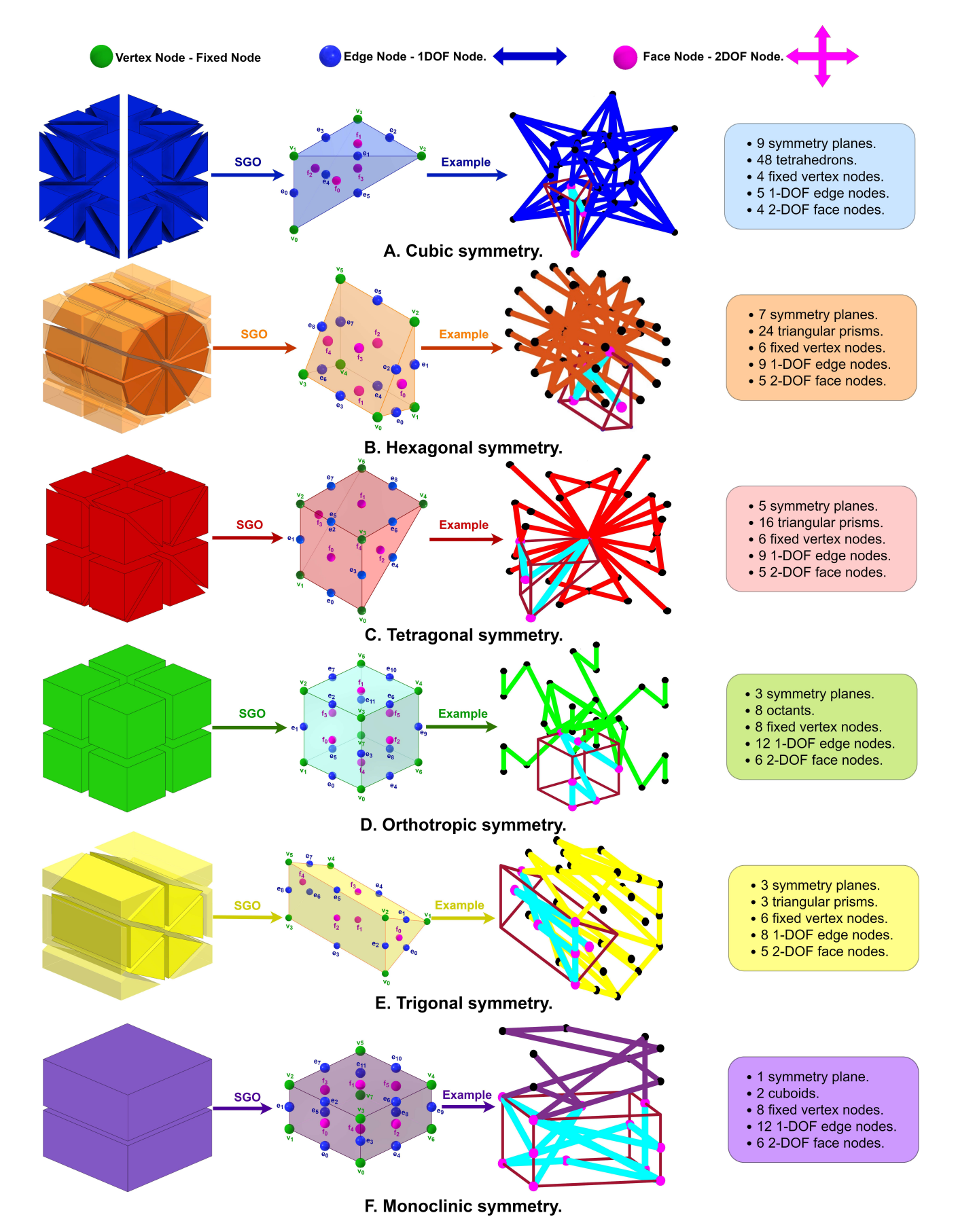


FIGURE 1: TRUSS STRUCTURE DESIGN LOGIC WITH DIFFERENT SYMMETRIES: A. CUBIC SYMMETRY, B. HEXAGONAL SYMMETRY, C. TETRAGONAL SYMMETRY, D. ORTHOTROPIC SYMMETRY, E. TRIGONAL SYMMETRY, AND F. MONOCLINIC SYMMETRY.

partition the cube into a specific number of symmetric geometric objects (SGOs), as illustrated in Figure 1. This approach allows us to define only a portion of the truss within a single SGO, simplifying the exploration search problem complexity while ensuring substantial flexibility and periodic tilability. Next, we apply reflection along the planes of symmetries to achieve the final topology with elastic characteristics resembling the type of symmetry used in constructing the truss topology. Within each SGO, the pattern's topology is defined by a set of edges connected with predefined nodes; these nodes can be vertex nodes, edge nodes, or face nodes. While there is a possibility to define an internal node, we have excluded it from our work as it does not offer additional coverage of the design space. Note that for triclinic materials, where there is no symmetry, it won't be mentioned in Figure 1. However, the method for obtaining highly anisotropic unit-cells will be discussed in Section 5.

Figure 1 lists Symmetric Geometric Objects (SGOs) resulting from dividing the cubic representative volume element (RVE) using symmetry planes determined by each material symmetry type. In cubic material, we have employed nine symmetry planes: three perpendicular to the primary cube axes and six perpendicular to the bisector of each pair of the primary three axes. These nine planes divide the cube into 48 symmetric tetrahedrons. For hexagonal material, seven symmetry planes are utilized. Six of these planes have normals lying in the same plane, forming 60° angles with each other. The seventh plane contains the normals to the other six, dividing the cube into 24 segments. These segments initially contain non-symmetric parts, which are subsequently removed to shape symmetric triangular prisms. Although alternative geometries can describe the SGO, we have chosen simplicity in shape by choosing triangular prisms. In tetragonal material, five symmetry planes are used: three perpendicular to the primary cube axes and the other two perpendicular to the bisector of the first and third primary cube axes. Tetragonal symmetry partitions the cube into 16 symmetric triangular prisms. Orthotropic materials feature three perpendicular planes of symmetry that are perpendicular to the primary axes of the cube. These three planes divide the cube into eight symmetric octants. Similar to orthotropic materials but with different symmetry planes' orientations, trigonal symmetry features three symmetry planes, with their normals all lying in the same plane and making angles of 120° with each other. The application of planes of symmetry in trigonal material results in six parts; we have modified them to achieve symmetry by excluding some non-symmetric parts and also some symmetric portions to simplify the resulting SGO. Consequently, the six resulting SGOs take the form of triangular prisms. The last material symmetry we have utilized is Monoclinic symmetry, where only one plane of symmetry is perpendicular to the third primary axis of the cube. This symmetry divides the cube into two cuboids.

It can be seen from Figure 1 that the positioning of vertex nodes, edge nodes, and face nodes within each SGO. While the vertex node remains fixed in its motion, edge, and face nodes are permitted restricted movement only along the edge and within

the face, respectively. The interconnection between the different nodes within each SGO defines the initial topologies of the truss dataset. Subsequently, adjustments in the offsets of the nodes capable of movement within their restricted regions are made to broaden the space of properties achievable by such datasets. Figure 2 provides examples of possible topologies generated from varying the sharing nodes or the offsets within a single prism.

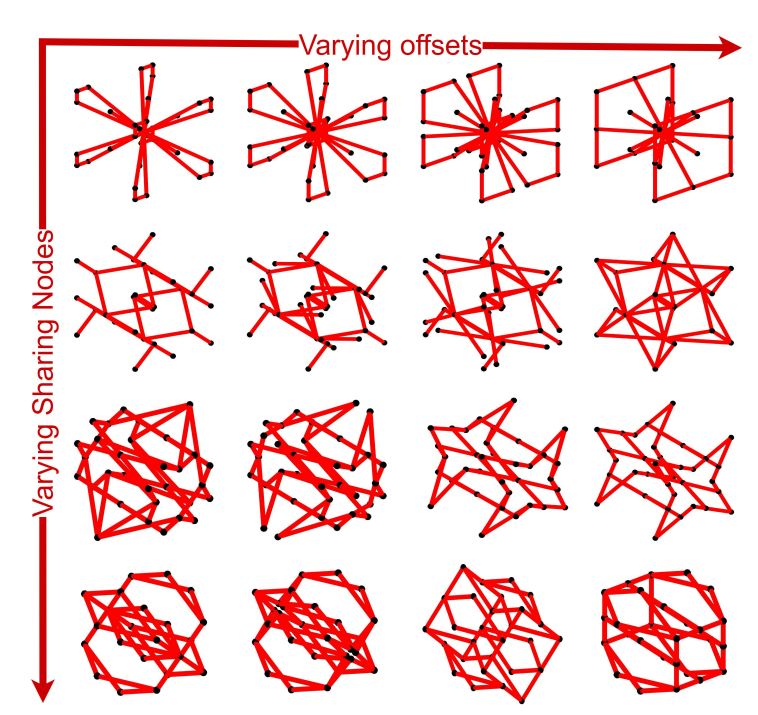


FIGURE 2: TETRAGONAL TOPOLOGIES ARE GENERATED THROUGH THE VARIATION OF BOTH THE SHARING NODES AND THE OFFSETS WITHIN A BASIC SGO (TRIANGULAR PRISM).

3.2 Continuity and Connectivity

One of the novelties of the proposed design approach is the dual representation of resulting topologies, allowing for representations in either parametric or graph form. In both representations, two types of variables are present: discrete and continuous. The discrete variables are symbolized by the selected nodes shared in the topology, while the continuous variables are illustrated by the positioning of the nodes within each SGO. We have constrained both types of variables to ensure the connectivity of the truss structures resulting from the symmetries. Additionally, we ensure that free-to-move nodes, particularly edge and face nodes, are positioned within their designated spatial bounds. Otherwise, this might violate the desired symmetries.

We define the offsets of nodes by taking inspiration from the shape function from the finite element community by utilizing the natural coordinate system [44], representing their relative positions with respect to the fixed vertex nodes.

The spatial position of each edge node finds its expression through the relative positions of the two vertex nodes that delineate the edge. Figure 3-A provides an insightful visualization of this representation. In Figure 3-A, let $pos(e_m)$, $pos(v_i)$, and $pos(v_j)$ be position vectors in \mathbb{R}^3 representing nodes e_m , v_i , and v_i , respectively. The position of node e_m adheres to the definition

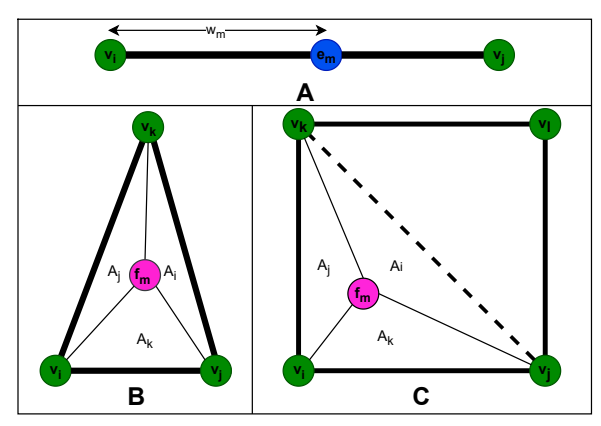


FIGURE 3: NATURAL COORDINATE SYSTEM FOR: A. EDGE NODE, B. FACE NODE ENCLOSED WITHIN A 2D PLANE OF 3 VERTEX NODES, AND C. FACE NODE ENCLOSED WITHIN A 2D PLANE OF 4 VERTEX NODES.

outlined in Eq. (2):

$$pos(e_{m}) = w_{m} pos(v_{i}) + (1 - w_{m}) pos(v_{i})$$
 (2)

where w_m stands as a weight parameter within the range $0 \le w_m \le 1$, exerting influence over the contribution of both v_i and v_j to the positional determination of e_m .

The face node can reside on a plane constrained between three or four vertex nodes, as depicted in Figure 3-B and Figure 3-C, respectively. Note that determining the face node's position on the plane requires only three vertex nodes. This positional determination leverages barycentric coordinates, a set of three scalar values that represent the weights of the vertices of a triangle in the formation of a given point within that triangle. As illustrated in Figure 3-B, $pos(f_m)$, $pos(v_i)$, $pos(v_j)$, and $pos(v_k)$ are position vectors in \mathbb{R}^3 representing nodes f_m , v_i , v_j , and v_k , respectively. The position of node f_m adheres to the formulation in Eq. (3):

$$pos(f_m) = w_{mi} pos(v_i) + w_{mj} pos(v_j) + w_{mk} pos(v_k)$$
 (3)

where w_{mi} , w_{mj} , and w_{mk} are the barycentric weights within the range $0 \le w_{mi}$, w_{mj} , $w_{mk} \le 1$. Figure 3-B illustrates that each weight corresponds to the area portion of the triangle resulting from the subdivision of the main plane triangle into three smaller ones by connecting the vertex nodes with the face node, where $w_{mn} = A_n/A$. Therefore, to ensure the placement of node f_m within the borders of the triangular region, it is essential that $\sum_{n=1}^3 w_{mn} = 1$. If the face node is intended to reside within the 2D plane constrained by four vertex nodes, the determination of its position involves dividing the plane into two triangular regions. Subsequently, the conditions of the barycentric coordinates within each triangular region are examined. If either of the regions satisfies the stipulated conditions, then the node is situated on the constrained plane defined by the four vertex nodes.

While the former addresses the positioning of nodes on their designated spatial bound defined by vertex nodes, the latter introduces the possibility of disconnected trusses or the emergence of a two-dimensional shape after applying the reflections on the symmetry planes. We addressed the second issue by examining

the coordinates of the resulting nodes after applying the reflection on symmetry planes. If there is no change in the positioning of any of the coordinates, it indicates that the structure lies within a 2D plane. Fortunately, the inherent symmetries prevent the resulting topology from lying on an inclined 2D plane. In the rare occurrence of 2D topologies, they consistently align with one of the three planes perpendicular to the primary axis of the topology.

The primary issue that may arise is expressed in the form of unconnected topologies, a concern evident in the dataset presented by Lumpe and Stankovic [1]. Connected topologies, depicted in Figure 4-B, signify the presence of a path linking all nodes sharing the unit-cell topology construction. Conversely, if there is no apparent finite path between any two nodes within the geometry, as illustrated in Figure 4-A, we can infer that the resulting structures are not connected.

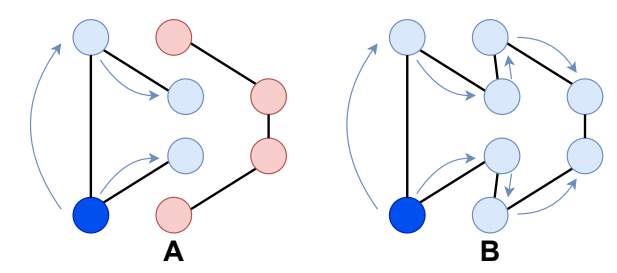


FIGURE 4: 2D VISUAL INSPECTION OF GRAPH CONNECTIVITY: A. UNCONNECTED GRAPH, AND B. CONNECTED GRAPH.

The connectivity is addressed as follows in our dataset generation: we expressed the topology using an adjacency matrix $A_d \in \{0,1\}^{n \times n}$, where n represents the number of nodes resulting from the unit-cell. In the adjacency matrix, a value of 1 denotes an edge between nodes, while 0 indicates the absence of an edge, which means the diagonal elements $A_{ii} = 1$ (for all $i=1,\ldots,n$) where n is the number of the nodes in the resulted unit-cell. Utilizing the adjacency matrix facilitates a connectivity check, which is achievable by examining the eigenvalues of the Laplacian matrix L, as defined by Eq. (4) [45].

$$L = D - A_d \tag{4}$$

where D is a diagonal matrix of vertex degrees, and A_d is the adjacency matrix. Let the Laplacian eigenvalues follow the order $\lambda_1 \leq \lambda_2 \leq \lambda_3 \leq ... \leq \lambda_n = 0$. If the second lowest eigenvalue is greater than zero $(\lambda_2 \geq 0)$, then the graph is algebraically connected [45]. The proposed method can effectively generate datasets for machine learning applications. However, the key question now is about the extent to which the property space can be covered by this method and whether it can explore regions that have not been explored before.

4. EFFECTIVE MATERIALS PROPERTIES SPACE

Exhaustively exploring the vast design space is impractical. A suitable sampling method is essential for probing the effective materials property space of the proposed structure design framework. In this work, we employed the Metropolis-Hastings Random Walk sampling technique [46]. In the realm of random walk sampling, the transition from one state to the next involves

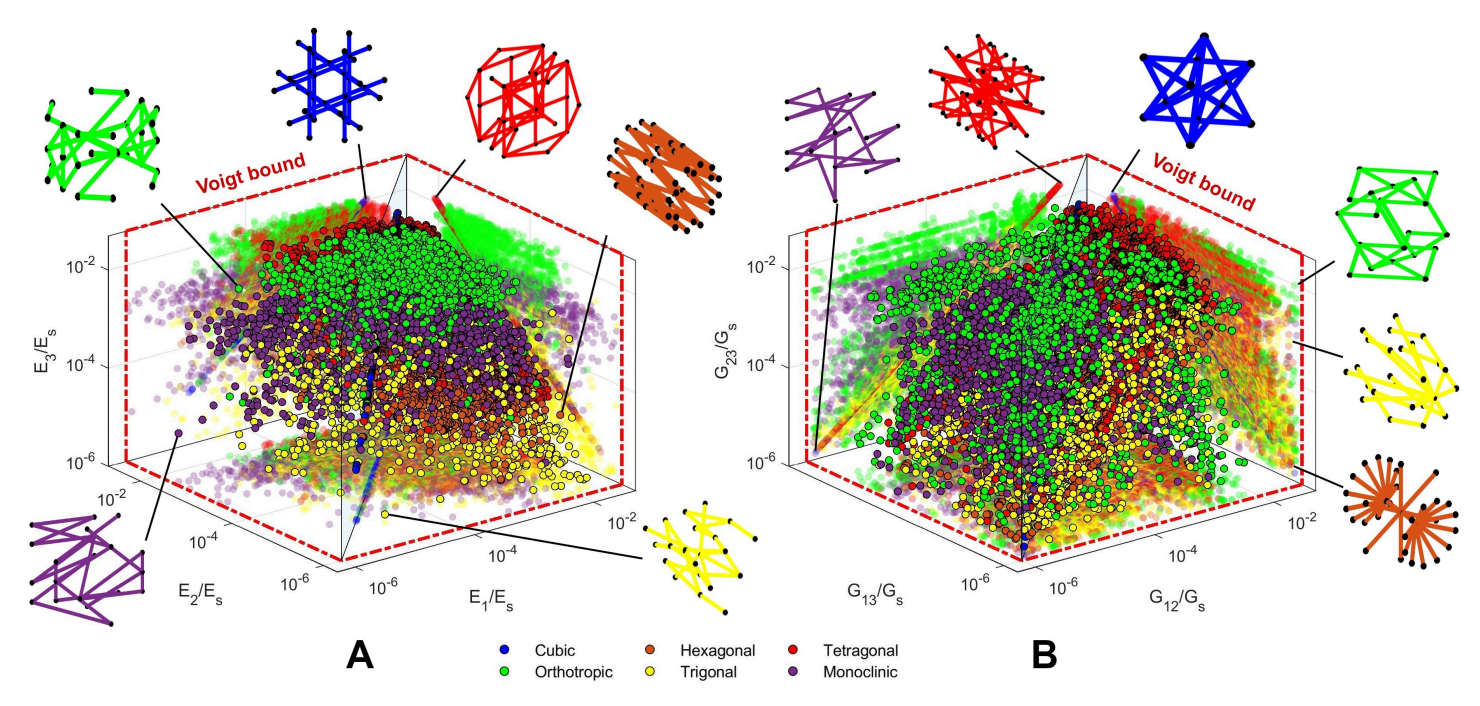


FIGURE 5: RELATIVE EFFECTIVE ELASTIC PROPERTIES OF ALL THE SYMMETRY METHODS FOR THE SAMPLED DATA: A. RELATIVE EFFECTIVE YOUNG'S MODULI IN THE THREE DIRECTIONAL PRIMARY AXES, AND B. RELATIVE EFFECTIVE SHEAR MODULI IN THE THREE DIRECTIONAL PRIMARY AXES.

randomly selecting one of the neighboring nodes. Defining which nodes as neighbors is a critical step. While it's conceivable to designate all nodes as neighbors, given the relatively modest number of nodes compared to larger graphs where this sampling method is typically applied, we opted for a random definition of node neighbors. Specifically, we employed the Erdős-Rényi Graph, assigning a 50% probability for any two nodes to be neighbors [47]. It's worth mentioning that we haven't extensively explored alternative sampling methods, as the primary focus of this work is to introduce the truss design framework, which will be in our future research.

We systematically sampled 2500 distinct topologies from each symmetry category, except for Cubic, where we sampled only 800 topologies, imposing a maximum relative density limit of 0.05 for all the symmetries. This constraint ensures a fair comparison of properties across diverse structures. Consequently, a varying number of nodes share within each SGO to achieve this relative density. Specifically, the number of sharing nodes ranges from 2 up to 3, 4, 5, 6, 7, and 12 for Cubic SGOs, Hexagonal SGOs, Tetragonal SGOs, Orthotropic SGOs, Triagonal SGOs, and Monoclinic SGOs respectively. Employing a numerical homogenization approach discussed previously [41], we compute the linear-elastic effective material properties for all structures. The underlying solid base material assumes a Young's modulus (E_s) of 200 GPa, a Poisson's ratio (ν s) of 0.3, and a truss diameter of 0.025. To gauge the property range of the truss structures within the samples and identify topologies with extreme mechanical behavior, we calculate and visually represent the homogenized relative effective Young's moduli, shear moduli, and Poisson's ratios of all 3D unit-cells.

Figure 5-A and Figure 5-B reveal the logarithmic scale rep-

resentation of the relative effective Young's moduli (E/E_s) and relative effective shear moduli (G/G_s) along the three directional primary coordinates 1, 2, 3, and projected onto the 12 plane, 23 plane, and 13 plane, respectively. The properties exhibit a wide range covering several orders of magnitude, ranging between 10^{-6} and 10^{-2} in the three directions. The red dashed–dotted lines denote the Voigt bounds, serving as theoretical maximums for Young's modulus and shear modulus, which can be determined by the base materials' elastic modulus and relative densities ($E_{Voigt} = \overline{\rho} \, E_s$ and $G_{Voigt} = \overline{\rho} \, G_s$) [48]. Given the density of data across different categories in the figure, we have included a separate space of properties for each symmetry type at the end of Appendix A, Figure A1, for vivid visualization purposes.

Cubic symmetry method establishes a linkage across all three directional primary axes, which is evident by the effective Young's and shear moduli that exhibit similar properties in all directions. Similarly, both hexagonal and tetragonal materials manifest two equal properties in two out of the three primary directions, suggesting a direct linkage between at least two of the primary axes of the main truss. However, the Orthotropic, Trigonal, and Monoclinic truss materials show no linkage in the directional Young's and shear moduli. The majority of samples from Cubic, Hexagonal, Tetragonal, and Orthotropic categories are frequently located in regions characterized by large threedirectional Young's moduli. However, the versatility of utilizing symmetry planes in the design process extends to regions where structures exhibit extreme compliance in one, two, or all three directions, as observed in some of the Triagonal and Monoclinic categories. The Triagonal and Monoclinic topologies are positioned closer to the boundary of the projected property space compared to other trusses resulting from the other symmetries.

In symmetries featuring planes that are inclined with respect to the primary axes of the cube (Cubic, Hexagonal, Tetragonal, and Trigonal), the directions of maximum stiffness do not always align with the primary axes. Diagonal planes may result in diagonal bars that directly stiffen the structures in the main shear directions, as depicted in Figure 5-B and the shear moduli figures in Appendix A.

For a comprehensive assessment of the materials properties' gamut of our method, a crucial step involves comparing them with the extensive dataset provided by Lumpe and Stankovic [1]. Following the same input parameters (200 GPa Young's Modulus base material, 0.3 Poisson's ratio, and 0.025 truss diameter), we computed the linear-elastic effective material properties for the entire catalog using the same numerical homogenization method. Subsequently, we excluded structures with relative densities exceeding 0.05, a constraint pertinent to the current study. This process resulted in the selection of 12,208 topologies from the catalog. Upon comparing the homogenized effective Young's moduli and shear moduli, as illustrated in Figure A2 in Appendix A, it becomes evident that a considerable portion of structures from the Lumpe and Stankovic dataset resides on or near the region where two or three directional properties are directly linked by structural symmetries. However, our symmetry plane method exhibits a broader span by expanding to regions where there is no direct linkage between directional stiffnesses or where structures demonstrate extreme compliance in one, two, or all three primary directions.

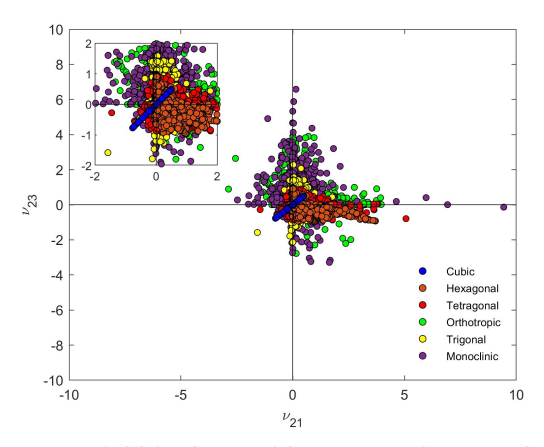


FIGURE 6: POISSON'S RATIOS ν_{21},ν_{23} FOR ALL SAMPLES ACROSS VARIOUS SYMMETRY METHODS AND A DETAILED VIEW OF THE RANGE $-2 \le \nu \le 2$.

Figure 6 displays the Poisson's ratios (ν_{21} and ν_{23}) for all samples across various symmetry methods (additional directions in Figure A3 in Appendix A). The results align with existing literature, indicating that an increase in anisotropy, signifying fewer symmetry planes, correlates with a higher likelihood of structures exhibiting extreme elastic behavior [49]. The Poisson's ratio range for cubic materials is confined to $-0.77 \le \nu_{21}, \nu_{23} \le 0.49$. In contrast, the range for monoclinic materials ranges between $-2.479 \le \nu_{21} \le 9.4$ and $-3.28 \le \nu_{23} \le 6.58$, reflecting the absence of a defined limit for the Poisson's ratio of 3D anisotropic unit-cells, as reported in [50]. This observation emphasizes the diverse behavior exhibited by different symmetry materials in

terms of Poisson's ratios.

The preceding exploration of the property space predominantly involved combinations of different nodes within each SGO, considering all types of nodes as fixed nodes. However, owing to the tileability of the unit-cell, wherein edge and face nodes exhibit characteristics that allow their continuous representation within their designated spatial bounds, an expansion of the property space becomes feasible. Specifically focused on the tetragonal samples, we have selected unit-cells from the boundaries of the Young's moduli space of properties. Subsequently, we made slight adjustments to the positions of the movable nodes, generating up to 50 new samples from each structure, as illustrated in Figure 7. This showcases an expanded property space while concurrently preserving the tetragonal behavior of the new topologies. Figure 7 provides a visual representation of the sharing nodes within each prism from the chosen topologies and the designated movement range. It is noteworthy that the applied movement is subtle, not exceeding 0.1 of the weight of the natural coordinate system in each direction. While a higher movement might lead to a broader dispersion of data points, it is certain that they would remain within the Voigt bound. This section has illuminated a segment of the property space, emphasizing the potential for broader exploration through increased sampling and simulations.

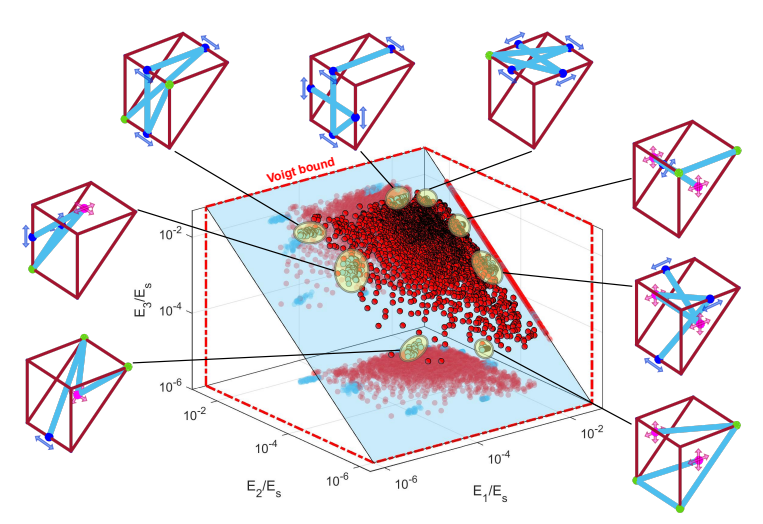


FIGURE 7: RELATIVE EFFECTIVE YOUNG'S MODULI ARE DEPICTED FOR BOTH THE ORIGINAL TETRAGONAL MATERIAL SAMPLES AND THE ALTERED NODES' POSITIONS WITHIN SELECTED TOPOLOGIES FROM THE TETRAGONAL SAMPLES. ADDITIONALLY, THE SGO (PRISM OF EACH CHOSEN UNIT-CELL) IS ILLUSTRATED, PROVIDING INSIGHT INTO THE DESIGNATED RANGE OF POSITION ADJUSTMENTS.

5. INTRODUCING ANISOTROPY

Our exploration investigates introducing anisotropy within symmetric planes, a critical facet that enhances the versatility of truss structures. The fundamental concept revolves around any geometric modification capable of influencing symmetries within the constructed topology, thereby inducing anisotropy [51]. To maintain a consistent dataset in this endeavor, we assume the use of the same material, truss diameter, and cross-section

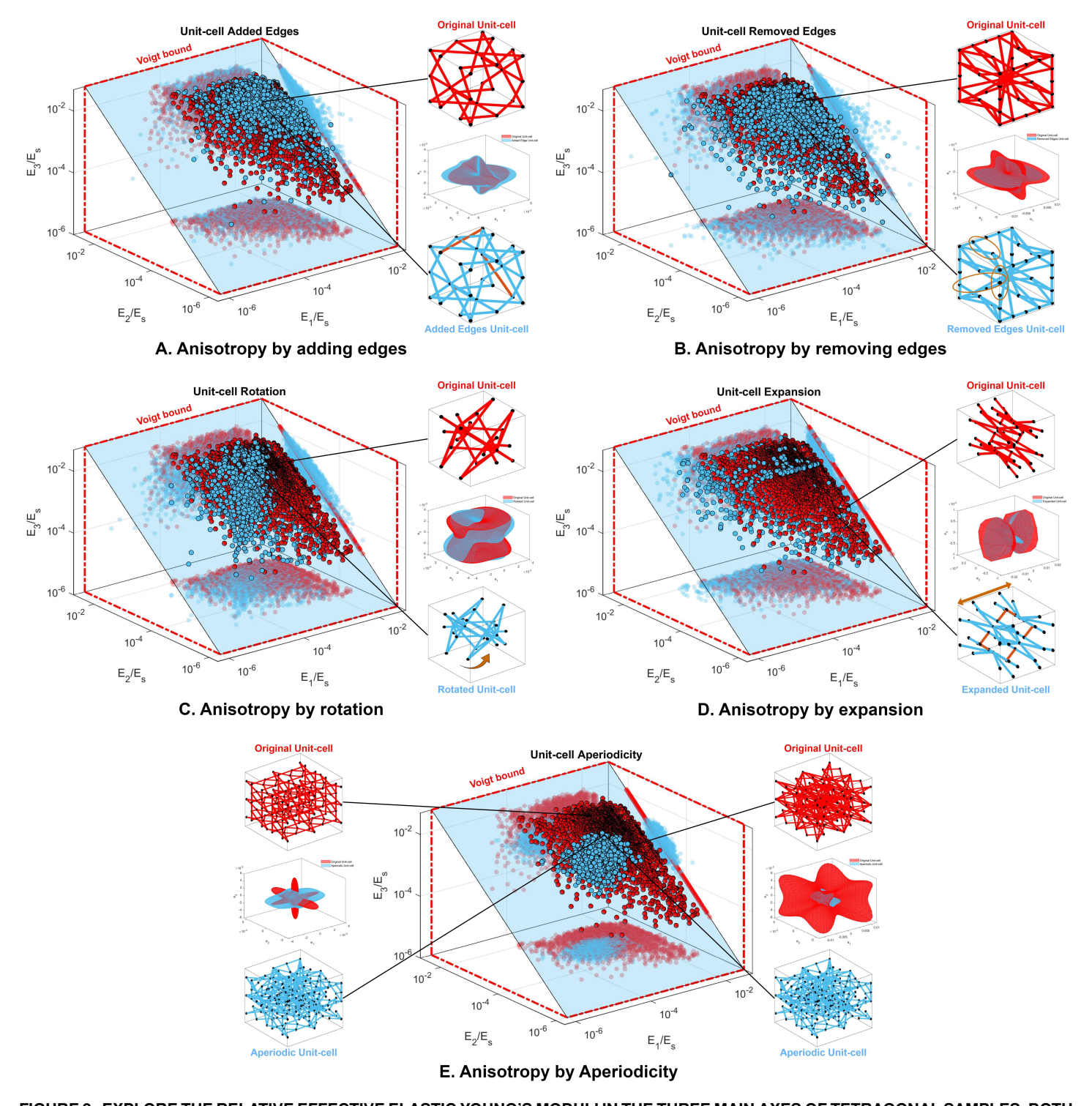


FIGURE 8: EXPLORE THE RELATIVE EFFECTIVE ELASTIC YOUNG'S MODULI IN THE THREE MAIN AXES OF TETRAGONAL SAMPLES, BOTH BEFORE AND AFTER APPLYING ANISOTROPY METHODS. ALSO, DISCOVER THE EFFECTIVE YOUNG'S MODULUS FOR A RANDOMLY CHOSEN TOPOLOGY BEFORE AND AFTER EMPLOYING THE FOLLOWING ANISOTROPY TECHNIQUES: A. ANISOTROPY BY ADDING EDGES, B. ANISOTROPY BY REMOVING EDGES, C. ANISOTROPY BY ROTATION, D. ANISOTROPY BY EXPANSION, AND E. ANISOTROPY BY APERIODICITY.

across each unit-cell, recognizing their substantial contributions to anisotropy, particularly in how they can be distributed or localized within a single unit-cell. Our focus lies primarily on the following key aspects: the addition or removal of a truss from the

final topology, expanding the length along one dimension, applying rotation, and joining different unit-cells in an aperiodic manner. When applied to the 2500 samples of the tetragonal material, these methods illustrate the diverse ways in which anisotropy can

be introduced. The specifics of these five distinct methods for introducing anisotropy are detailed as follows.

Adding edges to the symmetric unit-cell alters its symmetry. Therefore, we randomly added three new edges, connecting random points as depicted in Figure 8-A. This has resulted in a transformed stiffness tensor, now characterized by 21 independent elastic coefficients (Triclinic), in contrast to the conventional 6 or 7 of tetragonal material, indicating highly anisotropic topologies. Intuitively, the resulting topologies after adding the edges generally enhance stiffness in the direction where they are added, as observed in Figure 8-A.

Removing edges also introduces anisotropy to the symmetric unit-cells. We randomly deleted three edges from the symmetric unit-cells, as depicted in Figure 8-B. Similar to adding edges, removing edges resulted in a highly anisotropic stiffness tensor characterized by 21 independent parameters. The resulting topologies, after removing the edges, cause increased compliance, indicating reduced stiffness in the direction of the deleted truss.

Rotation serves as a fundamental technique, enabling the controlled reorientation of truss elements within symmetric planes. In our approach, we rotated all tetragonal samples by 15° around the axis defined by directional cosines ($I_1 = -0.5$, $I_2 = 0.35$, and $I_3 = 0.79$), as seen in Figure 8-C. The impact on the stiffness tensor mimics that of previous anisotropy methods, yielding a triclinic stiffness tensor following the rotation [52]. Notably, if the six load cases from the homogenization method are reoriented in alignment with the new orientation of the topology, the resulting stiffness tensor reverts to a tetragonal configuration. Hence, designers can leverage rotation to strategically position and orient the topology for optimal design outcomes.

Expansion of the topology represents another avenue for anisotropy introduction; in this process, we have expanded the dimensions along the first primary axis by 50% for all sampled data, which can be seen from Figure 8-D. Typically, expansion eliminates symmetries arising from inclined planes. However, if the planes of symmetry align perpendicularly to the primary axes of the topology, these symmetries remain preserved. In the case of the tetragonal material, the resulting topologies, after applying the expansions, exhibit orthotropic symmetries.

Aperiodicity serves as a more intricate approach involves the combination of different unit-cells to craft a new structure. While aperiodicity can manifest through various methods like gradation, perturbation, and hybridization [53], our focus here is solely on hybridization for the sake of maintaining consistency in the topologies. We established an 8-fold periodic unit-cell incorporating eight distinct topologies from the tetragonal samples, where v₀ serves as one of the sharing nodes of the SGO. This choice facilitates ease of connectivity between different unit-cells. The construction involved random generation of 2500 8-fold unitcells, each showcasing anisotropy. In Figure 8-E, we depict two of the unit-cells sharing the randomly illustrated 8-fold unit-cell. The illustration showcases how the effective Young's modulus varies upon superimposing different unit-cells and highlights the markedly different behavior under the same load conditions in the resultant structure.

In summary, our pursuit of introducing anisotropy within

symmetric planes encompasses versatile methods; each method serves as a source in tailoring truss structures to exhibit desired anisotropic characteristics, expanding the design space for advanced engineering applications.

6. DISCUSSIONS AND CONCLUSION

In our pursuit of advancing mechanical metamaterials and engineering, the role of material symmetries is pivotal in tailoring topologies with a diverse range of material properties. These symmetries serve as a design rational, particularly for cellular materials such as truss materials. Our truss material design method, inspired by six material symmetries (Cubic, Hexagonal, Tetragonal, Orthotropic, Trigonal, and Monoclinic), has proven to be a versatile and innovative approach. The foundation of our methodology lies in dividing a cube into symmetric SGOs using planes of symmetry related to each type of symmetry. Within each SGO, we define part of the truss material by connecting edges between predefined nodes. The defined sub-truss undergoes reflection on the symmetry planes, resulting in the creation of the final topology. To ensure structural connectivity and guarantee the formation of a three-dimensional topology, this topology undergoes two steps of constraints. The suggested design framework enables the description of truss material in representations suitable for machine learning methods, such as parametric and graph representations. Our exploration of the property space of the proposed method showcases its ability to achieve a diverse range of mechanical properties, even with a limited number of samples. This surpasses even the most extensive truss datasets in the literature. Moreover, introducing five anisotropy methods—bar addition, bar deletion, topology rotation, topology expansion, and aperiodicity—further enhances the versatility of our approach. These anisotropy introduction methods not only provide avenues for tailoring specific mechanical characteristics but also contribute to the comprehensiveness of our design framework.

Looking forward, there are exciting directions for future research. A more refined sampling method could potentially yield a more exhaustive exploration of the property space, building upon the success of our current methodology. Additionally, extending the application of our method beyond truss structures to generate other cellular materials, such as defining curved bars or full surfaces within each SGO, holds promise for even greater diversity and broader applications. This opens up new horizons for the development of advanced materials with tailored properties for various engineering and design applications.

ACKNOWLEDGMENT

We acknowledge the support of NSF CMMI-2245298 and NASA #80MSFC23M0001.

REFERENCES

- [1] Lumpe, Thomas S. and Stankovic, Tino. "Exploring the property space of periodic cellular structures based on crystal networks." *Proceedings of the National Academy of Sciences* Vol. 118 No. 7 (2021): p. e2003504118.
- [2] Panetta, Julian, Zhou, Qingnan, Malomo, Luigi, Pietroni, Nico, Cignoni, Paolo and Zorin, Denis. "Elastic textures

- for additive fabrication." *ACM Trans. Graph.* Vol. 34 No. 4 (2015).
- [3] Sunada, Toshikazu. "Lecture on topological crystallography." *Japanese Journal of Mathematics* Vol. 7 (2012): pp. 1–39.
- [4] Hyde, Bruce G. *Crystal Structures: Patterns and symmetry*. Mineralogical Society of America (1996).
- [5] Greaves, George Neville, Greer, A Lindsay, Lakes, Roderic S and Rouxel, Tanguy. "Poisson's ratio and modern materials." *Nature materials* Vol. 10 No. 11 (2011): pp. 823–837.
- [6] Wagner, Marius A., Lumpe, Thomas S., Chen, Tian and Shea, Kristina. "Programmable, active lattice structures: Unifying stretch-dominated and bending-dominated topologies." Extreme Mechanics Letters Vol. 29 (2019): p. 100461.
- [7] Meza, Lucas R., Phlipot, Gregory P., Portela, Carlos M., Maggi, Alessandro, Montemayor, Lauren C., Comella, Andre, Kochmann, Dennis M. and Greer, Julia R. "Reexamining the mechanical property space of three-dimensional lattice architectures." *Acta Materialia* Vol. 140 (2017): pp. 424–432.
- [8] Portela, Carlos M., Greer, Julia R. and Kochmann, Dennis M. "Impact of node geometry on the effective stiffness of non-slender three-dimensional truss lattice architectures." Extreme Mechanics Letters Vol. 22 (2018): pp. 138–148.
- [9] Paulose, Jayson, Meeussen, Anne S. and Vitelli, Vincenzo. "Selective buckling via states of self-stress in topological metamaterials." *Proceedings of the National Academy of Sciences* Vol. 112 No. 25 (2015): pp. 7639–7644.
- [10] Abu-Mualla, Mohammad, Jiron, Victor and Huang, Jida. "Inverse Design of Two-Dimensional Shape-Morphing Structures." *Journal of Mechanical Design* Vol. 145 No. 12 (2023): p. 121703.
- [11] Qu, Jingyuan, Gerber, Alexander, Mayer, Frederik, Kadic, Muamer and Wegener, Martin. "Experiments on Metamaterials with Negative Effective Static Compressibility." *Phys. Rev. X* Vol. 7 (2017): p. 041060.
- [12] Bückmann, Tiemo, Thiel, Michael, Kadic, Muamer, Schittny, Robert and Wegener, Martin. "An elasto-mechanical unfeelability cloak made of pentamode metamaterials." *Nature communications* Vol. 5 No. 1 (2014): p. 4130.
- [13] Kumar, S, Ubaid, J, Abishera, R, Schiffer, A and Deshpande, VS. "Tunable energy absorption characteristics of architected honeycombs enabled via additive manufacturing." *ACS applied materials & interfaces* Vol. 11 No. 45 (2019): pp. 42549–42560.
- [14] Guell Izard, Anna, Bauer, Jens, Crook, Cameron, Turlo, Vladyslav and Valdevit, Lorenzo. "Ultrahigh Energy Absorption Multifunctional Spinodal Nanoarchitectures." Small Vol. 15 No. 45 (2019): p. 1903834.
- [15] Chen, Yanyu, Li, Tiantian, Scarpa, Fabrizio and Wang, Lifeng. "Lattice Metamaterials with Mechanically Tunable Poisson's Ratio for Vibration Control." *Phys. Rev. Appl.* Vol. 7 (2017): p. 024012.
- [16] Li, Ying, Baker, Evan, Reissman, Timothy, Sun, Cheng and Liu, Wing Kam. "Design of mechanical metamaterials

- for simultaneous vibration isolation and energy harvesting." *Applied Physics Letters* Vol. 111 No. 25 (2017): p. 251903.
- [17] Watts, Seth, Arrighi, William, Kudo, Jun, Tortorelli, Daniel A and White, Daniel A. "Simple, accurate surrogate models of the elastic response of three-dimensional open truss micro-architectures with applications to multiscale topology design." *Structural and Multidisciplinary Optimization* Vol. 60 (2019): pp. 1887–1920.
- [18] Xu, Shanqing, Shen, Jianhu, Zhou, Shiwei, Huang, Xiaodong and Xie, Yi Min. "Design of lattice structures with controlled anisotropy." *Materials Design* Vol. 93 (2016): pp. 443–447.
- [19] Chougrani, Laurent, Pernot, Jean-Philippe, Véron, Philippe and Abed, Stéphane. "Parts internal structure definition using non-uniform patterned lattice optimization for mass reduction in additive manufacturing." *Engineering with Computers* Vol. 35 No. 1 (2019): pp. 277–289.
- [20] Azizi, Mahdi, Aickelin, Uwe, Khorshidi, Hadi A. and Shishehgarkhaneh, Milad Baghalzadeh. "Shape and size optimization of truss structures by Chaos game optimization considering frequency constraints." *Journal of Advanced Research* Vol. 41 (2022): pp. 89–100.
- [21] Sigmund, Ole. "A new class of extremal composites." *Journal of the Mechanics and Physics of Solids* Vol. 48 No. 2 (2000): pp. 397–428.
- [22] Chen, Desai, Skouras, Mélina, Zhu, Bo and Matusik, Wojciech. "Computational discovery of extremal microstructure families." *Science Advances* Vol. 4 No. 1 (2018): p. eaao7005.
- [23] Bastek, Jan-Hendrik, Kumar, Siddhant, Telgen, Bastian, Glaesener, Raphaël N. and Kochmann, Dennis M. "Inverting the structure–property map of truss metamaterials by deep learning." *Proceedings of the National Academy of Sciences* Vol. 119 No. 1 (2022): p. e2111505119.
- [24] Maurizi, Marco, Gao, Chao and Berto, Filippo. "Inverse design of truss lattice materials with superior buckling resistance." *npj Computational Materials* Vol. 8 No. 1 (2022): p. 247.
- [25] Abu-Mualla, Mohammad and Huang, Jida. "Inverse design of 3D cellular materials with physics-guided machine learning." *Materials Design* Vol. 232 (2023): p. 112103.
- [26] Zheng, Li, Karapiperis, Konstantinos, Kumar, Siddhant and Kochmann, Dennis M. "Unifying the design space and optimizing linear and nonlinear truss metamaterials by generative modeling." *Nature Communications* Vol. 14 No. 1 (2023): p. 7563.
- [27] Mao, Huina, Rumpler, Romain and Göransson, Peter. "An inverse method for characterisation of the static elastic Hooke's tensors of solid frame of anisotropic open-cell materials." *International Journal of Engineering Science* Vol. 147 (2020): p. 103198.
- [28] Mao, Huina, Rumpler, Romain, Gaborit, Mathieu, Göransson, Peter, Kennedy, John, O'Connor, Daragh, Trimble, Daniel and Rice, Henry. "Twist, tilt and stretch: From isometric Kelvin cells to anisotropic cellular materials." *Materials Design* Vol. 193 (2020): p. 108855.

- [29] Al Sabouni-Zawadzka, Anna. "Extreme Mechanical Properties of Regular Tensegrity Unit Cells in 3D Lattice Metamaterials." *Materials* Vol. 13 No. 21 (2020).
- [30] Li, Zuyu, Gao, Wei, Yu Wang, Michael, Wang, Chun H. and Luo, Zhen. "Three-dimensional metamaterials exhibiting extreme isotropy and negative Poisson's ratio." *International Journal of Mechanical Sciences* Vol. 259 (2023): p. 108617.
- [31] Chen, Xueyan, Moughames, Johnny, Ji, Qingxiang, Martínez, Julio Andrés Iglesias, Tan, Huifeng, Adrar, Samia, Laforge, Nicolas, Cote, Jean-Marc, Euphrasie, Sébastien, Ulliac, Gwenn, Kadic, Muamer and Laude, Vincent. "Optimal isotropic, reusable truss lattice material with near-zero Poisson's ratio." Extreme Mechanics Letters Vol. 41 (2020): p. 101048.
- [32] Sigmund, Ole. "Tailoring materials with prescribed elastic properties." *Mechanics of Materials* Vol. 20 No. 4 (1995): pp. 351–368.
- [33] Ha, Chan Soo, Yao, Desheng, Xu, Zhenpeng, Liu, Chenang, Liu, Han, Elkins, Daniel, Kile, Matthew, Deshpande, Vikram, Kong, Zhenyu, Bauchy, Mathieu et al. "Rapid inverse design of metamaterials based on prescribed mechanical behavior through machine learning." *Nature Communications* Vol. 14 No. 1 (2023): p. 5765.
- [34] Makatura, Liane, Wang, Bohan, Chen, Yi-Lu, Deng, Bolei, Wojtan, Chris, Bickel, Bernd and Matusik, Wojciech. "Procedural Metamaterials: A Unified Procedural Graph for Metamaterial Design." ACM Trans. Graph. Vol. 42 No. 5 (2023).
- [35] Shubnikov, Alekseĭ. "Symmetry in science and art.".
- [36] Cowin, Stephen C. *Continuum mechanics of anisotropic materials*. Springer Science & Business Media (2013).
- [37] Cowin, S. C. and Mehrabadi, M. M. "Anisotropic Symmetries of Linear Elasticity." *Applied Mechanics Reviews* Vol. 48 No. 5 (1995): pp. 247–285.
- [38] Latture, Ryan M., Begley, Matthew R. and Zok, Frank W. "Design and mechanical properties of elastically isotropic trusses." *Journal of Materials Research* Vol. 33 No. 3 (2018): p. 249–263.
- [39] Rastegarzadeh, Sina, Muthusamy, Samuel and Huang, Jida. "Mechanical Profile of Smooth Cellular Materials." *Journal of Manufacturing Science and Engineering* Vol. 145 No. 2 (2022): p. 021005.
- [40] Chadwick, Peter, Vianello, Maurizio and Cowin, Stephen C. "A new proof that the number of linear elastic symmetries is eight." *Journal of the Mechanics and Physics of Solids* Vol. 49 No. 11 (2001): pp. 2471–2492. The Jean-Paul Boehler Memorial Volume.
- [41] Dong, Guoying, Tang, Yunlong and Zhao, Yaoyao Fiona. "A 149 Line Homogenization Code for Three-Dimensional Cellular Materials Written in matlab." *Journal of Engineering Materials and Technology* Vol. 141 No. 1 (2018): p. 011005.
- [42] Bensoussan, Alain, Lions, Jacques-Louis and Papanicolaou, George. *Asymptotic analysis for periodic structures*. Vol. 374. American Mathematical Soc. (2011).

- [43] Hill, R. "The Elastic Behaviour of a Crystalline Aggregate." *Proceedings of the Physical Society. Section A* Vol. 65 No. 5 (1952): p. 349.
- [44] Bi, Zhuming. Finite element analysis applications: a systematic and practical approach. Academic Press (2017).
- [45] Fiedler, Miroslav. "Algebraic connectivity of graphs." *Czechoslovak mathematical journal* Vol. 23 No. 2 (1973): pp. 298–305.
- [46] Qi, Xiao. "A Review: Random Walk in Graph Sampling." (2022).
- [47] ERDdS, P and R&wi, A. "On random graphs I." *Publ. math. debrecen* Vol. 6 No. 290-297 (1959): p. 18.
- [48] Meyers, Marc André and Chawla, Krishan Kumar. *Mechanical behavior of materials*. Cambridge university press (2008).
- [49] Lethbridge, Zoe A.D., Walton, Richard I., Marmier, Arnaud S.H., Smith, Christopher W. and Evans, Kenneth E. "Elastic anisotropy and extreme Poisson's ratios in single crystals." *Acta Materialia* Vol. 58 No. 19 (2010): pp. 6444–6451.
- [50] Ting, T. C. T. and Chen, Tungyang. "Poisson's ratio for anisotropic elastic materials can have no bounds." *The Quarterly Journal of Mechanics and Applied Mathematics* Vol. 58 No. 1 (2005): pp. 73–82.
- [51] Vannucci, Paolo and Vannucci, Paolo. *General anisotropic elasticity*. Springer (2018).
- [52] Bond, Walter L. "The mathematics of the physical properties of crystals." *The Bell System Technical Journal* Vol. 22 No. 1 (1943): pp. 1–72.
- [53] Ramirez-Chavez, Irving E., Anderson, Daniel, Sharma, Raghav, Lee, Christine and Bhate, Dhruv. "A Classification of Aperiodic Architected Cellular Materials." *Designs* Vol. 6 No. 4 (2022).

APPENDIX A. PROPERTIES DESIGN SPACE EXTRA FIGURES

This appendix includes some of the space of properties figures mentioned in the paper's context

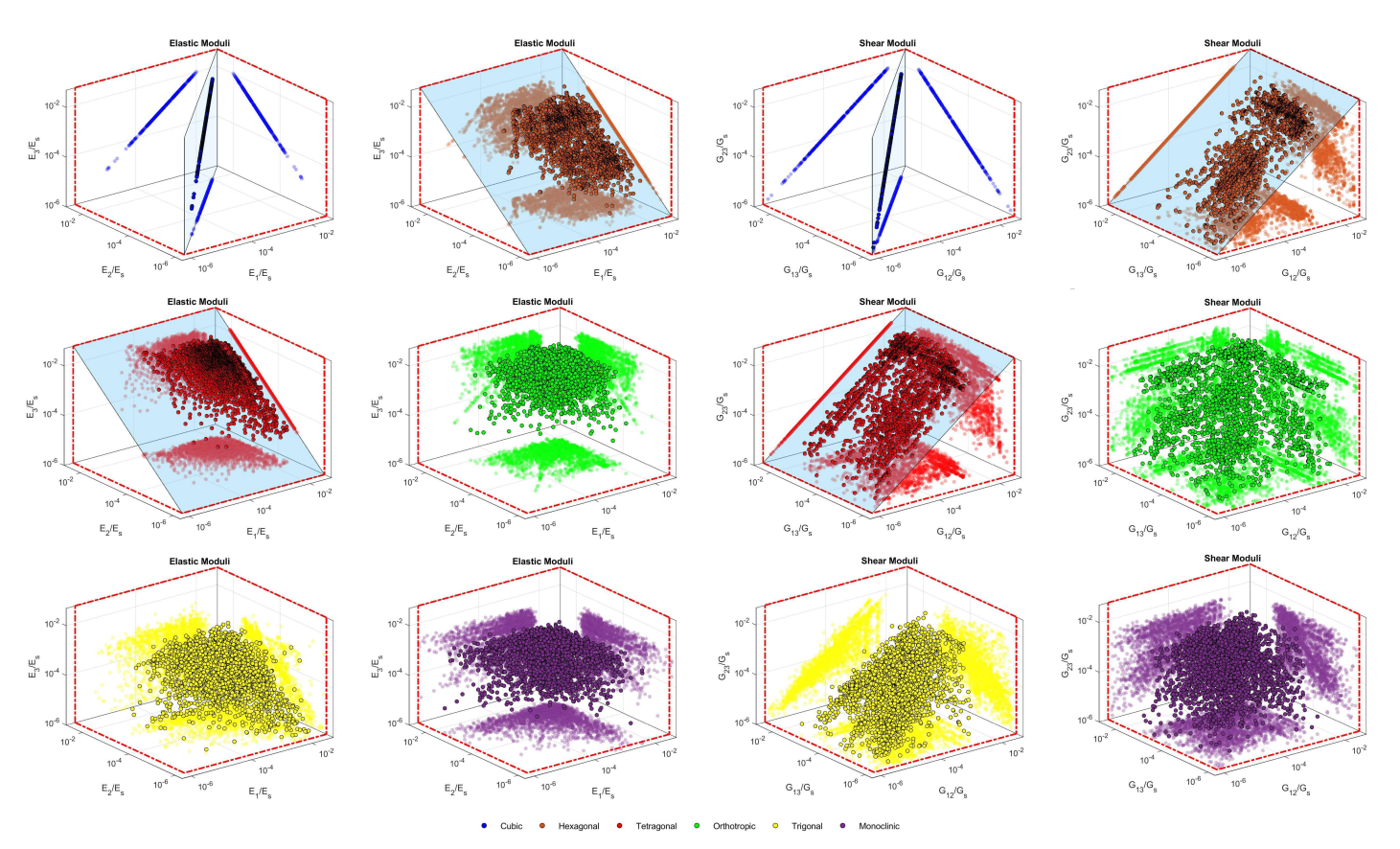


FIGURE A1: RELATIVE EFFECTIVE YOUNG'S MODULI AND EFFECTIVE SHEAR MODULI OF ALL THE SYMMETRY METHODS FOR THE SAMPLED DATA.

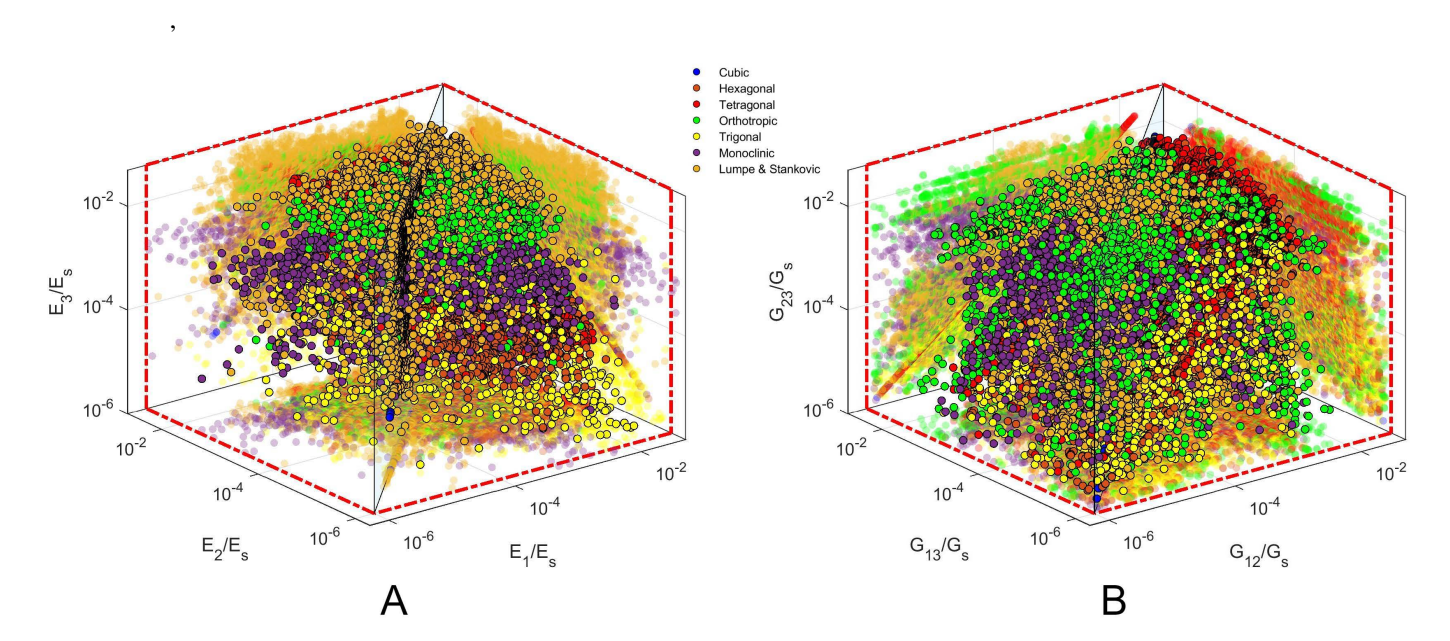


FIGURE A2: COMPARISON BETWEEN THE LUMPE AND STANKOVIC DATASET AND THE SAMPLE OF THE PROPOSED PLANE OF SYMMETRY DESIGN METHOD IN TERMS OF EFFECTIVE ELASTIC MECHANICAL PROPERTIES: A. RELATIVE EFFECTIVE YOUNG'S MODULI IN THE THREE DIRECTIONAL PRIMARY AXES, AND B. RELATIVE EFFECTIVE SHEAR MODULI IN THE THREE DIRECTIONAL PRIMARY AXES.

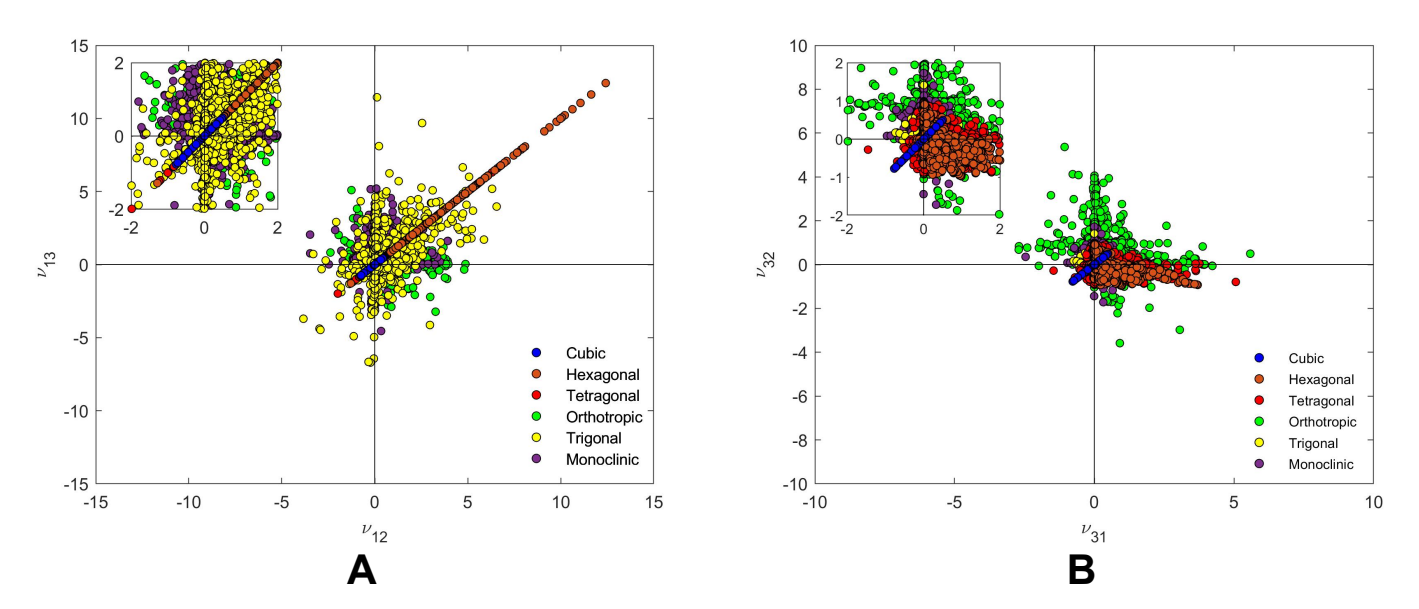


FIGURE A3: POISSON'S RATIOS FOR ALL SAMPLES ACROSS VARIOUS SYMMETRY METHODS AND A DETAILED VIEW OF THE RANGE $-2 \le \nu \le 2$ FOR A. ν_{12}, ν_{13} , AND B. ν_{31}, ν_{32} .